Analog Quantum Control of Magnonic Cat States on a Chip by a Superconducting Qubit

Kounalakis, Marios; Bauer, Gerrit E.W.; Blanter, Yaroslav M.

DOI
10.1103/PhysRevLett.129.037205

Publication date
2022

Document Version
Final published version

Published in
Physical Review Letters

Analog Quantum Control of Magnonic Cat States on a Chip by a Superconducting Qubit

Marios Kounalakis,[1,*] Gerrit E. W. Bauer,[2,1,3] and Yaroslav M. Blanter[1]
[1]Kavli Institute of Nanoscience, Delft University of Technology, 2628 CJ Delft, Netherlands
[2]WPI-AIMR, Tohoku University, 2-1-1, Katahira, Sendai 980-8577, Japan
[3]Kavli Institute for Theoretical Sciences, University of the Chinese Academy of Sciences, 100190 Beijing, China

(Received 27 March 2022; accepted 22 June 2022; published 13 July 2022)

We propose to directly and quantum-coherently couple a superconducting transmon qubit to magnons—the quanta of the collective spin excitations, in a nearby magnetic particle. The magnet's stray field couples to the qubit via a superconducting quantum interference device. We predict a resonant magnon-qubit exchange and a nonlinear radiation-pressure interaction that are both stronger than dissipation rates and tunable by an external flux bias. We additionally demonstrate a quantum control scheme that generates magnon-qubit entanglement and magnonic Schrödinger cat states with high fidelity.

DOI: 10.1103/PhysRevLett.129.037205

Introduction.—Quantum magnonics is a rapidly growing field of research on magnetic devices operating in the quantum realm [1]. Magnons, i.e., the quanta of the collective spin excitations in magnetic materials [2–5], in the high-quality magnet yttrium iron garnet (YIG) couple strongly with microwave photons in superconducting resonators, i.e., with coupling rates far exceeding the system decay rates [6–8]. Quantum coherence of a macroscopic number of spins has been achieved by indirectly coupling a YIG sphere with a superconducting qubit in a microwave cavity [9–12]. Magnon-photon coupling has also been demonstrated in optical setups, enabling microwave-optical transducers at the quantum level [13–16]. These results establish magnons, along with phonons and photons, as promising carriers of quantum information in emerging hybrid quantum technologies [17–19].

An important milestone toward the realization of quantum devices is the ability to prepare and manipulate nonclassical states of the many-spin system, that are strongly entangled, squeezed, or display negative Wigner functions [20,21], which may be expected in driven magnon-photon systems [22]. The macroscopic superpositions of coherent states or "Schrödinger cat" states [23] are especially attractive as essential building blocks for continuous-variable quantum information tasks, e.g., in fault-tolerant quantum computing [24–27], quantum communication [28,29], and quantum simulation [30], as well as for quantum metrology [31–33] and fundamental studies of the quantum-to-classical transition [34,35]. While such states can be prepared in superconducting cavities [25–29] and potentially in micromechanical resonators [36–39], magnetic systems offer a number of attractive and unique functionalities such as integration into spintronic circuits, unidirectional magnon propagation, as well as chiral couplings to phonons and photons [40–43].

Recent theoretical proposals address the realization of such states in magnonic devices. In the optical domain, magnonic cat states could be prepared by pulsed sideband driving [44], however, this requires a much stronger coupling than appears possible to date. Creating such states in an ellipsoid ferromagnet inside a microwave cavity might be possible, but is hindered by the requirement of collapsing the cavity field in a high-photon-number state [45]. Quantum states of a driven ferromagnet can be generated in a cavity when resonantly coupled to a qubit [46] following protocols from cavity and circuit quantum electrodynamics [47,48] based on the digital quantum computing paradigm of sequential qubit operations (quantum gates) [49,50]. However, cumulative gate errors as well as long gate operation times hinder the preparation of macroscopic quantum superpositions. In addition, despite their flexibility, digital schemes are very demanding on resources, compared to more robust analog approaches [51]. It is therefore desirable to develop *analog* schemes to prepare and control quantum states in which the system evolves under natural interactions without clocked external operations.

Here, we propose a hybrid device comprising a YIG particle directly coupled to a planar superconducting qubit via magnetic stray fields, which can additionally be used to synthesize high-fidelity magnonic cat states by analog means. The direct magnon-qubit flux-mediated interaction is sufficiently strong at practical distances such that a mediating microwave cavity is not needed. Moreover, the interaction can be tuned *in situ*, providing a lot of flexibility in constructing artificial magnonic quantum networks [52]. Specifically, the system features two distinct and tunable couplings. First, we find a resonant magnon-qubit exchange interaction, akin to the Jaynes-Cummings model [9,53], which can be used to create quantum states by digital protocols [46,47]. Second, we find a strong and

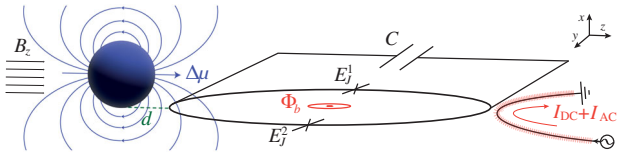

FIG. 1. Proposed circuit architecture. A YIG particle with uniform magnetization oriented by an in-plane field B_z close to a flux-tunable transmon qubit, formed by a SQUID loop and a capacitor C in parallel. The magnetic fluctuations $\Delta\mu$ induce a flux in the SQUID that modulates its inductive energy and therefore the qubit frequency. An external flux bias Φ_b can be applied locally via control lines carrying dc and ac currents.

nonlinear interaction analogous to the radiation-pressure in optomechanics [54–56], which has never been explored in magnon-qubit systems before. We demonstrate that this coupling can be resonantly enhanced by dynamically driving the qubit to generate robust quantum superpositions of coherent states in a purely analog fashion, with a fidelity that is limited only by the magnon lifetime.

The device.—The superconducting element in our circuit is a flux-tunable transmon qubit [57], i.e., a superconducting quantum interference device (SQUID) shunted by a capacitor C, as depicted in Fig. 1. The former is a superconducting loop interrupted by two Josephson junctions, with Josephson energies E_J^1 and E_J^2. Its inductive energy depends nonlinearly on the superconducting phase difference $\hat{\delta}$ and an externally applied flux Φ_b [58],

$$\mathcal{E}_{\rm ind}(\hat{\delta},\phi_b) = -E_J^{\rm max} S(\phi_b)\cos\left[\hat{\delta} - \arctan\left(a_J\tan\phi_b\right)\right], \quad (1)$$

where $\phi_b \doteq \pi\Phi_b/\Phi_0$, $S(\phi_b) = \sqrt{\cos^2\phi_b + a_J^2\sin^2\phi_b}$, and the imbalance between the Josephson energies or SQUID asymmetry $a_J = |E_J^1 - E_J^2|/E_J^{\rm max}$ is an important design parameter (see below), with $E_J^{\rm max} \doteq E_J^1 + E_J^2$.

The transmon is described by the Hamiltonian $\hat{H}_0^T = 4E_C\hat{N}^2 + \mathcal{E}_{\rm ind}(\hat{\delta},\Phi_b)$, where $E_C = e^2/(2C)$ is the charging energy and $\hat{N}$ (operator conjugate to $\hat{\delta}$) represents the number of tunneling Cooper pairs [59]. The operators $\hat{N},\hat{\delta}$ can be expressed in terms of bosonic annihilation (creation) operators $\hat{c}^{(\dagger)}$ [59],

$$\hat{N} = iN_{\rm zpf}(\hat{c}^\dagger - \hat{c}), \qquad \hat{\delta} = \delta_{\rm zpf}(\hat{c} + \hat{c}^\dagger), \quad (2)$$

where $N_{\rm zpf} = [E_J^{\rm max}S(\phi_b)/(32E_C)]^{1/4}$ and $\delta_{\rm zpf} = \{2E_C/[E_J^{\rm max}S(\phi_b)]\}^{1/4}$. In the transmon regime $[E_J^{\rm max}S(\phi_b) \gg E_C]$, $\hat{H}_0^T = \hbar\omega_q\hat{c}^\dagger\hat{c} - (E_C/2)\hat{c}^\dagger\hat{c}^\dagger\hat{c}\,\hat{c}$, where $\hbar\omega_q = \sqrt{8E_CE_J^{\rm max}S(\phi_b)} - E_C$ is the transmon excitation energy and the second (self-Kerr) nonlinear term defines the anharmonicity $-E_C$ [57].

The magnet is a YIG particle, without loss of generality chosen here to be a sphere with radius $R_{\rm YIG}$, placed at an in-plane center-to-center distance $d + R_{\rm SQUID}$ from the SQUID, as depicted in Fig. 1. An in-plane magnetic field $B_z\hat{\mathbf{z}}$ orients the magnetization $\mathbf{M}$ or spin angular momentum $\mathbf{S} = -(4/3)\pi R_{\rm YIG}^3\mathbf{M}/\gamma_0$, where γ_0 is the modulus of the gyromagnetic ratio [5]. The fundamental excitation is a uniform precession or Kittel mode with ferromagnetic resonance frequency $\omega_m = \gamma_0(B_z + B_{\rm ani})$, where $B_{\rm ani}$ is the anisotropy field [60].

The Hamiltonian of the magnetic order can be mapped on a quantum harmonic oscillator by the leading term of the Holstein-Primakoff expansion in terms of bosonic operators $m^{(\dagger)}$ that create (annihilate) a magnon [5]. Omitting the zero-point energy $\hbar\omega_m/2$, a weakly excited Kittel mode is well described by $\hat{H}_0^M = \hbar\omega_m\hat{m}^\dagger\hat{m}$ [5]. The amplitudes of the magnetic excitations are $\Delta\hat{\mu}_x = \mu_{\rm zpf}(\hat{m} + \hat{m}^\dagger)$, $\Delta\hat{\mu}_y = i\mu_{\rm zpf}(\hat{m} - \hat{m}^\dagger)$, and $\Delta\hat{\mu}_z = \hbar\gamma_0\hat{m}^\dagger\hat{m}$, where $\mu_{\rm zpf} = \hbar\gamma_0\sqrt{N_S/2}$, and N_S is the total number of spins.

The magnetic moment emits a stray field $\mathbf{B}_{\rm YIG}$ that induces a flux through the SQUID loop, thereby modulating its inductive energy and the qubit frequency. According to Eq. (1) by $\phi_b \to \phi_b + \phi(\Delta\hat{\boldsymbol{\mu}})$ [see Supplemental Material [61] for the derivation],

$$\mathcal{E}_{\rm ind}(\hat{\delta},\phi_b,\Delta\hat{\boldsymbol{\mu}}) = -sE_J^{\rm max}\{[\cos\phi_b - \phi(\Delta\hat{\boldsymbol{\mu}})\sin\phi_b]\cos\hat{\delta} + a_J[\sin\phi_b + \phi(\Delta\hat{\boldsymbol{\mu}})\cos\phi_b]\sin\hat{\delta}\}, \quad (3)$$

where $s \doteq \mathrm{sgn}[\cos\phi_b]$ for $\phi(\Delta\hat{\boldsymbol{\mu}}) \ll 1$, noting that $\phi(\Delta\hat{\boldsymbol{\mu}}) \lesssim 10^{-3}$ for typical parameters. We thus arrive at a total Hamiltonian, $\hat{H} = \hat{H}_0^M + \hat{H}_0^T + \hat{H}_{\rm int}$ with

$$\hat{H}_{\rm int} = \frac{E_J^{\rm max}\phi(\Delta\hat{\boldsymbol{\mu}})}{S(\phi_b)}\left[\frac{\sin 2\phi_b}{2}(1-a_J^2)\cos\hat{\tilde{\delta}} - a_J\sin\hat{\tilde{\delta}}\right], \quad (4)$$

where $\hat{\tilde{\delta}} \doteq \hat{\delta} - \arctan(a_J\tan\phi_b)$.

In the far-field limit the induced flux reads

$$\phi(\Delta\hat{\boldsymbol{\mu}}) = \iint \mathbf{B}_{\rm YIG}(\Delta\hat{\boldsymbol{\mu}})d\mathbf{A} = \frac{\mu_0}{4\Phi_0 d_{\rm min}}\sum_{i=x,y,z} I_i\Delta\hat{\mu}_i, \quad (5)$$

where A is the loop area, $d_{\rm min} = \sqrt{R_{\rm YIG}^2 + d^2}$ and $I_x, I_y, I_z = \mathcal{O}(1)$ are dimensionless geometrical factors. For a point magnetic dipole, in the limit of a large loop radius, and assuming $d = R_{\rm YIG}$ ($d_{\rm min} = \sqrt{2}R_{\rm YIG}$) we have $I_y = 0$, $I_x \simeq -1$ [52], therefore,

$$\phi(\Delta\hat{\boldsymbol{\mu}}) = -\frac{\mu_0\mu_{\rm zpf}}{4\Phi_0 d_{\rm min}}(\hat{m} + \hat{m}^\dagger). \quad (6)$$

Note that we disregarded the magnon number fluctuations since $\hbar\gamma_0 \ll \mu_{\rm zpf}$ for $N_S \gg 1$.

Expanding to order $\tilde{\delta}^2$ in Eq. (4) and using Eqs. (2) and (6), the interaction reads

$$\hat{H}_{\rm int}/\hbar = J(\hat{c}^\dagger \hat{m} + \hat{c}\hat{m}^\dagger) + g_{\rm rp}\hat{c}^\dagger\hat{c}(\hat{m} + \hat{m}^\dagger), \quad (7)$$

where we disregarded fast-rotating terms $(\hat{c}^\dagger)^n \hat{m}^{(\dagger)}$ (rotating-wave approximation) because $J, g_{\rm rp} \ll \omega_{q,m}$. Terms of $\mathcal{O}[\hat{\delta}^4]$ in Eq. (4) lead to interactions that are irrelevant in the qubit manifold, but cause small corrections to $g_{\rm rp}$ and J [61].

Magnon-qubit couplings.—The first term in Eq. (7),

$$J = \frac{\mu_0\mu_{\rm zpf}}{4d_{\rm min}\Phi_0}\frac{a_J[2E_C(E_J^{\rm max})^3]^{1/4}}{\hbar[S(\phi_b)]^{5/4}}, \quad (8)$$

describes the coherent exchange between qubit and magnon excitations, similar to the Jaynes-Cummings model of light-matter interaction [53] and the effective magnon-qubit coupling in cavities [9]. The nonlinear term in Eq. (7) has a coupling strength

$$g_{\rm rp} = \frac{\mu_0\mu_{\rm zpf}}{16d_{\rm min}\Phi_0}\frac{\sqrt{8E_J^{\rm max}E_C}(1-a_J^2)\sin 2\phi_b}{\hbar[S(\phi_b)]^{3/2}}, \quad (9)$$

similar to the radiation pressure in optomechanical systems [67] or the optical photon-magnon coupling [13].

In Fig. 2 we plot both coupling strengths as a function of the applied flux Φ_b and SQUID asymmetry a_J, including higher-order corrections [61]. We assume typical transmon parameters $E_J^{\rm max}/h = 50$ GHz, $E_C/h = 200$ MHz, and YIG radius $R_{\rm YIG} = 3$ μm leading to $N_S = 2.4\times10^{12}$ for typical densities [9]. J has a maximum at $\phi_b = \pi/2$, vanishes for a fully symmetric SQUID ($a_J = 0$) and approaches a constant when highly asymmetric. While here, we assumed that the junction capacitances are the same, in the Supplemental Material we treat the more general case including a finite capacitance asymmetry and find that $J = 0$ when one junction vanishes ($a_J = 1$), as expected [61]. On the other hand, $g_{\rm rp}$ changes sign at $\phi_b = \pi/2$ and vanishes for $a_J \to 1$. Both its maximal value and the optimal bias point depend on a_J, which is fixed by sample design and fabrication [68].

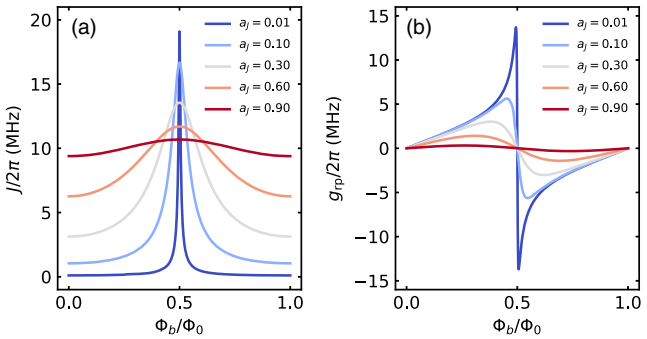

FIG. 2. Couplings vs flux bias. Coupling strength of the magnon-qubit exchange interaction J (a) and "photon-pressure" interaction $g_{\rm rp}$ (b) as a function of the applied flux bias Φ_b, for different values of the SQUID asymmetry α_J.

Quantum manipulations require operation in the strong coupling regime $J, g_{\rm rp} > \kappa, 1/T_{1,2}$, where $\kappa = \omega_m\alpha_G$ is the magnon decay rate in terms of the Gilbert damping constant α_G, while T_1 and T_2 are the transmon relaxation and dephasing times, respectively. As shown in Fig. 2(a), J is minimal at $\phi_b = k\pi (k\epsilon\mathbb{Z})$ where the qubit is insensitive to flux noise (see Fig. S1 [61]). However, highly asymmetric transmons operate equally well around the stationary points $\phi_b = (2k+1)\pi/2$, at the cost of a narrower tuning range [69]. The asymmetry parameter strikes a compromise between strong coupling, acceptable tuning range, and high coherence. For example, choosing $a_J = 0.6$ at $\phi_b = \pi/2$, we have $J/(2\pi) \gtrsim 10$ MHz, therefore the system is in the strong coupling regime with $T_{1,2} \simeq 20$ μs [70] and typical Gilbert damping parameters $\alpha_G \sim 10^{-5}$–10^{-4} [5,9,71]. The interaction can be switched on and off easily by fast flux pulses shifting the qubit frequency [70] and algorithmic sequences of qubit control pulses may create arbitrary quantum states of magnons [46–48]. However, multiple qubit pulses propagate errors that can prevent the generation of a given state. Moreover, the finite pulse duration, typically around 10–100 ns [72], limits the number of operations that can be performed within the relaxation times. Given the relatively short magnon lifetime at GHz frequencies, ranging from hundreds of nanoseconds to a few microseconds [5,9,71], such digital schemes appear less attractive.

Rather than building magnon superpositions pulse by pulse, large cat states can be generated by the nonlinear radiation pressure, which couples magnonic displacements with qubit frequency shifts. This coupling, in the interaction picture $g_{\rm rp}\hat{c}^\dagger\hat{c}(\hat{m}e^{-i\omega_m t} + \hat{m}^\dagger e^{i\omega_m t})$, can be activated in the ultrastrong coupling regime $g_{\rm rp} \gtrsim \omega_m$ [37,56], or by applying a stroboscopic qubit pulse train with period $T = \pi/\omega_m$ and pulse duration $\ll T$ [73]. Alternatively, it may be activated in a tripartite configuration with an additional qubit, enabling arbitrary magnonic states via pulsed schemes [38]. However, these approaches encounter the difficulty that magnon frequencies are larger than 100 MHz $\gg g_{\rm rp}$, while qubit gates below 10 ns lead to interference of higher transmon levels [72]. Here, we propose to enhance the nonlinearity by a time-dependent modulation of the coupling as proposed for trapped ions and mechanical systems [74,75] based on a parametric flux modulation of the SQUID loop, which can be implemented by local control strip lines [76].

Cat state preparation protocol.—The coupling Eq. (9) reduces for a symmetric SQUID to $g_{\rm rp} = (\omega_p \sin\phi_b/\sqrt{|\cos\phi_b|})(\mu_0\mu_{\rm zpf}/8\Phi_0 d_{\rm min}) \to \omega_p(\mu_0\mu_{\rm zpf}\phi_{\rm ac}/8\Phi_0 d_{\rm min})\times\cos(\omega_{\rm ac}t)$, where in the second step we used a weak ac bias $\phi_b = \phi_{\rm ac}\cos(\omega_{\rm ac}t)$ ($\phi_{\rm ac} \ll 1$) and defined the Josephson plasma frequency $\omega_p = \sqrt{8E_J^{\rm max}E_C}/\hbar$. The Hamiltonian, in the rotating frame $\hat{U}(t) = e^{i\omega_{\rm ac}t\hat{m}^\dagger\hat{m}}$, reads

$$\hat{\tilde{H}} = \hat{U}^\dagger\hat{H}\,\hat{U} = \hat{H}_0^T + \hbar\delta\hat{m}^\dagger\hat{m} + \hbar\tilde{g}_{\rm rp}\hat{c}^\dagger c(\hat{m} + \hat{m}^\dagger), \quad (10)$$

with $\delta = (\omega_m - \omega_{\rm ac})$ and $\tilde{g}_{\rm rp} = (\mu_0 \mu_{\rm zpf} \phi_{\rm ac}/16\Phi_0 d_{\rm min})\omega_p$. Here, we employed the rotating wave approximation by omitting rapidly varying interaction terms $\tilde{g}_{\rm rp}\hat{c}^\dagger c\hat{m}^{(\dagger)} e^{\pm i2\omega_{\rm ac}t}$ $(2\omega_{ac} \gg \tilde{g}_{\rm rp})$ and assumed unperturbed qubit eigenstates since $\omega_{\rm ac} \ll \omega_q$. Flux modulation is experimentally well established [76] without requiring additional circuitry, in contrast with modulating E_C, $d_{\rm min}$, or $\mu_{\rm zpf}$. In the configuration of Fig. 1 the flux bias line and the magnet are spatially separated to minimize crosstalk. The remaining weak microwave field results in a slight coherent displacement of the magnon state, which does not perturb the interaction dynamics.

The resonant modulation $(\delta = 0)$ generates coherent magnon displacements conditioned by the qubit, leading to macroscopic quantum superpositions of magnetization by the following protocol. Starting with both systems in their ground state and applying a $R_{\hat{y},(\pi/2)}$ qubit pulse [70,77], creates the superposition state $|+\rangle_q = (|0\rangle_q + |1\rangle_q)/\sqrt{2}$. After turning on the modulation, the system evolves (according to $\hat{\tilde{H}}$) into $[|0\rangle_q|0\rangle_m + e^{i\theta(t)}|1\rangle_q|\beta(t)\rangle_m]/\sqrt{2}$, where $\beta(t) = (\tilde{g}_{\rm rp}/\delta)(e^{-i\delta t} - 1), \theta(t) = (\tilde{g}_{\rm rp}/\delta)^2(\delta t - \sin\delta t)$ [36]. Switching off the flux modulation at $t = \tau$ leaves the system in a highly entangled hybrid Bell-cat state [78] $\frac{1}{2}\{|+\rangle_q[|0\rangle + e^{i\theta(\tau)}|\beta(\tau)\rangle]_m + |-\rangle_q[|0\rangle - e^{i\theta(\tau)}|\beta(\tau)\rangle]_m\}$.

The protocol is concluded by applying a second $R_{\hat{y},(\pi/2)}$ rotation followed by a strong projective measurement that collapses the qubit state. If the measurement yields $|0\rangle_q$ $(|1\rangle_q)$ the magnet is left in a macroscopic superposition of coherent states, i.e., an even (odd) cat state $|\psi\rangle^{\rm even}_{\rm odd} = [|0\rangle_m \pm |\beta(\tau)\rangle_m]/\mathcal{N}$, where $\mathcal{N} = \sqrt{2}(1 \pm e^{-|\beta(t)|^2/2})^{1/2}$, and $\beta(\tau) = -i\tilde{g}_{\rm rp}\tau$ for $\delta \to 0$. Following a coherent magnon displacement of amplitude $-\beta(\tau)/2$ this state is equivalent to $[|-\beta(\tau)/2\rangle_m \pm |\beta(\tau)/2\rangle_m]/\mathcal{N}$, consisting of only even (odd) magnon number states.

We can model these operations by the quantum statistical Lindblad master equation [79] $\dot{\rho} = (i/\hbar)[\rho, \hat{\tilde{H}}] + \omega_m\alpha_G\{n_{\rm th}\mathcal{L}[\hat{m}^\dagger]\rho + (n_{\rm th}+1)\mathcal{L}[\hat{m}]\rho\} + (1/T_1)\mathcal{L}[\hat{c}]\rho + (1/T_2)\mathcal{L}[\hat{c}^\dagger\hat{c}]\rho$, where the superoperator $\mathcal{L}[\hat{o}]\rho = (2\hat{o}\rho\hat{o}^\dagger - \hat{o}^\dagger\hat{o}\rho - \rho\hat{o}^\dagger\hat{o})/2$ describes the bare dissipation channels, and $n_{\rm th} = 1/\{\exp[\hbar\omega_m/(k_B T)] - 1\}$ is the number of thermally excited magnons at temperature T. YIG's weak magnetic anisotropy $B_{\rm ani} = -2.5$ mT [71] enables working at sub-GHz frequencies with low magnon decay rates $\omega_m\alpha_G$ and weak magnetic fields. We chose $\omega_m/(2\pi) = 500$ MHz and $T = 5$ mK (for higher temperatures see [61]) and typical qubit relaxation and dephasing times $T_1 = T_2 = 20$ μs [72]. The required in-plane magnetic field ~20 mT does not compromise the qubit performance [80]. We model the transmon $\hat{H}_0^T$ as a three-level system with anharmonicity $-E_C$, although there is no leakage from the qubit subspace during the protocol, and solve the dynamics numerically in a basis of up to 140 magnon levels.

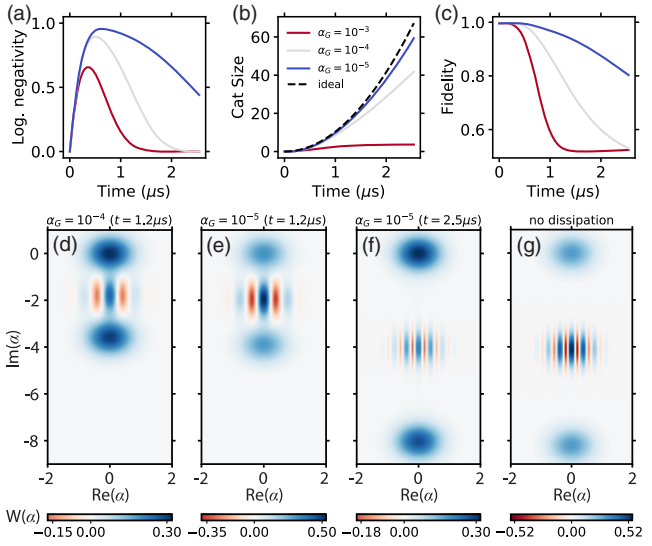

FIG. 3. Magnonic cat states. (a) Logarithmic negativity E_N showcasing the evolution of entanglement in the bipartite system for $10^{-5} \le \alpha_G \le 10^{-3}$. (b) Corresponding magnon cat size S, where the dashed curve plots the ideal case $S = |\tilde{g}_{\rm rp}t|^2$. (c) Fidelity of the prepared state to target $|\psi\rangle_{\rm even}$. Bottom row: Wigner function of prepared magnonic cats with fidelities $\mathcal{F} \ge 80\%$ for $\alpha_G = 10^{-4}$ (d), 10^{-5} (e),(f) and no dissipation (g), calculated at $t \simeq 1.2$ μs (d),(e) and $t \simeq 2.5$ μs (f),(g).

We benchmark our protocol for different values of the Gilbert damping parameter α_G, as shown in Fig. 3, using drive parameters $\phi_{\rm ac} = \pi/10$, $\omega_{\rm ac} = \omega_m$ and circuit parameters from Fig. 2. We first address the entanglement of the bipartite system by monitoring the evolution of the logarithmic negativity $E_N = \log_2[2N(\rho) + 1]$, where $N(\rho)$ is the sum of negative eigenvalues of the partial transpose of the joint density matrix ρ [81]. Figure 3(a) shows that after qubit initialization and evolution under $\hat{\tilde{H}}$, the magnon-qubit entanglement increases up to a maximum value ($E_N^{\rm max} = 1$ without dissipation) before the magnon decay takes over and eventually destroys it.

As explained above, collapsing the qubit in $|0\rangle_q$ prepares a magnonic even cat state. In Fig. 3(b) we plot the cat "size" $S = |\beta(t)|^2$, defined as the squared distance between the superposed coherent states in phase space [23,77]. Figure 3(c) shows the prepared state fidelity $\mathcal{F} = \sqrt{\langle\psi_{\rm even}|\rho_m|\psi_{\rm even}\rangle}$ [79,82], where ρ_m is the magnon density matrix after tracing out the qubit. We can visualize the cat state in terms of the Wigner quasiprobability distribution, $W(\alpha) = 2/\pi\,{\rm Tr}\{D^\dagger(\alpha)\rho_m D(\alpha)e^{i\pi\hat{m}^\dagger\hat{m}}\}$, where $D(\alpha) = e^{\alpha\hat{m}^\dagger - \alpha^*\hat{m}}$ is the magnon displacement operator [20]. In Figures 3(d)–3(f) we plot the Wigner function for $\alpha_G = 10^{-4}$ and $\alpha_G = 10^{-5}$, calculated at selected times

where $\mathcal{F} \simeq 80\%$ (d), (f) and $\mathcal{F} \simeq 95\%$ (e). Figure 3(g) shows the Wigner function at $t = 2.5$ μs for the dissipationless case. We clearly observe the characteristic quantum features of cat states, such as interference fringes with $W(\alpha) < 0$. It should therefore be possible to prepare high-fidelity large cat states with sizes $S \geq 40$ for realistic values of $10^{-5} \leq \alpha_G \leq 10^{-4}$ [5,9,71]. Our analysis holds for noninteracting magnons. When the total magnon number $\langle \hat{m}^\dagger \hat{m} \rangle = |\beta(t)|^2/2$ is much smaller than the total number of spins (N_S) magnon-magnon interactions are negligibly small [22]. In our setup corrections would be necessary when $|\tilde{g}_{\mathrm{rp}} t|^2/2 \sim N_S$. With parameters $\tilde{g}_{\mathrm{rp}}/(2\pi) \sim 0.5$ MHz and $N_S \sim 10^{12}$ pumping such magnon numbers takes seconds, which is orders of magnitude larger than their lifetime.

The quantum nature of the magnetic states can be verified by homodyne magnetization state tomography of $W(\alpha)$ [83] by combining ac spin pumping with inverse spin Hall voltage measurements. Wigner tomography can also be achieved by operating the magnon-qubit system in the strong dispersive regime, $J^2/(\omega_q - \omega_m) \gg \kappa,\ 1/T_1$, and using the transmon as a magnon detector [70,77,78]. Finally, rapid modulation of the radiation-pressure coupling combined with magnon displacement operations and qubit measurements can yield signatures of the prepared cat state [36]. The last two methods require a dispersively coupled microwave resonator to the qubit [84].

Conclusion.—Strong and tunable magnon-qubit couplings can be realized in a hybrid quantum system comprising a magnetized YIG sphere directly coupled via magnetic flux to a transmon qubit in a planar superconducting circuit. This architecture features both resonant magnon-qubit exchange as well as purely nonlinear interactions, in a flexible and compact geometry with *in situ* tunability. To the best of our knowledge, we are the first to propose a device that employs the direct interaction of magnons with superconducting qubits and, in particular, nonlinear magnon-qubit couplings of the radiation-pressure type. The intrinsic nonlinearity of both the transmon qubit and the radiation-pressure coupling empowers the creation of nontrivial quantum magnonic states even in the weak excitation regime, in which magnons behave as harmonic oscillators. We devised and tested an analog protocol that is particularly useful for the high-fidelity generation of large macroscopic quantum superpositions of magnetization under realistic experimental conditions. Our results enrich the quantum control toolbox in magnonic devices and open new possibilities for constructing artificial 2D quantum magnonic networks [52,85] or building magnonic analogs of the bosonic codes paradigm [24,27,86] with transmons playing the role of ancillary control elements.

We thank Christian Dickel and Mehrdad Elyasi for reading and commenting on the manuscript. This research was supported by the Dutch Foundation for Scientific Research (NWO) and the JSPS Kakenhi Grant No. 19H00645.

*marios.kounalakis@gmail.com, m.kounalakis@tudelft.nl

[1] A. V. Chumak *et al.*, IEEE Trans. Magn. **58**, 1 (2022).
[2] A. V. Chumak, V. I. Vasyuchka, A. A. Serga, and B. Hillebrands, Nat. Phys. **11**, 453 (2015).
[3] Y. Tabuchi, S. Ishino, A. Noguchi, T. Ishikawa, R. Yamazaki, K. Usami, and Y. Nakamura, C.R. Phys. **17**, 729 (2016).
[4] D. Lachance-Quirion, Y. Tabuchi, A. Gloppe, K. Usami, and Y. Nakamura, Appl. Phys. Express **12**, 070101 (2019).
[5] B. Z. Rameshti, S. V. Kusminskiy, J. A. Haigh, K. Usami, D. Lachance-Quirion, Y. Nakamura, C.-M. Hu, H. X. Tang, G. E. Bauer, and Y. M. Blanter, arXiv:2106.09312 [Phys. Rep.].
[6] H. Huebl, C. W. Zollitsch, J. Lotze, F. Hocke, M. Greifenstein, A. Marx, R. Gross, and S. T. B. Goennenwein, Phys. Rev. Lett. **111**, 127003 (2013).
[7] Y. Tabuchi, S. Ishino, T. Ishikawa, R. Yamazaki, K. Usami, and Y. Nakamura, Phys. Rev. Lett. **113**, 083603 (2014).
[8] X. Zhang, C.-L. Zou, L. Jiang, and H. X. Tang, Phys. Rev. Lett. **113**, 156401 (2014).
[9] Y. Tabuchi, S. Ishino, A. Noguchi, T. Ishikawa, R. Yamazaki, K. Usami, and Y. Nakamura, Science **349**, 405 (2015).
[10] D. Lachance-Quirion, Y. Tabuchi, S. Ishino, A. Noguchi, T. Ishikawa, R. Yamazaki, and Y. Nakamura, Sci. Adv. **3**, e1603150 (2017).
[11] S. P. Wolski, D. Lachance-Quirion, Y. Tabuchi, S. Kono, A. Noguchi, K. Usami, and Y. Nakamura, Phys. Rev. Lett. **125**, 117701 (2020).
[12] D. Lachance-Quirion, S. P. Wolski, Y. Tabuchi, S. Kono, K. Usami, and Y. Nakamura, Science **367**, 425 (2020).
[13] S. Viola Kusminskiy, H. X. Tang, and F. Marquardt, Phys. Rev. A **94**, 033821 (2016).
[14] X. Zhang, N. Zhu, C.-L. Zou, and H. X. Tang, Phys. Rev. Lett. **117**, 123605 (2016).
[15] A. Osada, R. Hisatomi, A. Noguchi, Y. Tabuchi, R. Yamazaki, K. Usami, M. Sadgrove, R. Yalla, M. Nomura, and Y. Nakamura, Phys. Rev. Lett. **116**, 223601 (2016).
[16] J. A. Haigh, A. Nunnenkamp, A. J. Ramsay, and A. J. Ferguson, Phys. Rev. Lett. **117**, 133602 (2016).
[17] G. Kurizki, P. Bertet, Y. Kubo, K. Mølmer, D. Petrosyan, P. Rabl, and J. Schmiedmayer, Proc. Natl. Acad. Sci. U.S.A. **112**, 3866 (2015).
[18] A. Clerk, K. Lehnert, P. Bertet, J. Petta, and Y. Nakamura, Nat. Phys. **16**, 257 (2020).
[19] H. Yuan, Y. Cao, A. Kamra, R. A. Duine, and P. Yan, Phys. Rep. **965**, 1 (2022).
[20] K. E. Cahill and R. J. Glauber, Phys. Rev. **177**, 1882 (1969).
[21] A. Kenfack and K. Życzkowski, J. Opt. B **6**, 396 (2004).
[22] M. Elyasi, Y. M. Blanter, and G. E. W. Bauer, Phys. Rev. B **101**, 054402 (2020).
[23] S. Deleglise, I. Dotsenko, C. Sayrin, J. Bernu, M. Brune, J.-M. Raimond, and S. Haroche, Nature (London) **455**, 510 (2008).
[24] M. Mirrahimi, Z. Leghtas, V. V. Albert, S. Touzard, R. J. Schoelkopf, L. Jiang, and M. H. Devoret, New J. Phys. **16**, 045014 (2014).
[25] N. Ofek, A. Petrenko, R. Heeres, P. Reinhold, Z. Leghtas, B. Vlastakis, Y. Liu, L. Frunzio, S. M. Girvin, L. Jiang, M. Mirrahimi, M. H. Devoret, and R. J. Schoelkopf, Nature (London) **536**, 441 (2016).

[26] S. Rosenblum, P. Reinhold, M. Mirrahimi, L. Jiang, L. Frunzio, and R. J. Schoelkopf, Science **361**, 266 (2018).

[27] C. Chamberland, K. Noh, P. Arrangoiz-Arriola, E. T. Campbell, C. T. Hann, J. Iverson, H. Putterman, T. C. Bohdanowicz, S. T. Flammia, A. Keller *et al.*, PRX Quantum **3**, 010329 (2022).

[28] K. S. Chou, J. Z. Blumoff, C. S. Wang, P. C. Reinhold, C. J. Axline, Y. Y. Gao, L. Frunzio, M. Devoret, L. Jiang, and R. Schoelkopf, Nature (London) **561**, 368 (2018).

[29] L. D. Burkhart, J. D. Teoh, Y. Zhang, C. J. Axline, L. Frunzio, M. H. Devoret, L. Jiang, S. M. Girvin, and R. J. Schoelkopf, PRX Quantum **2**, 030321 (2021).

[30] E. Flurin, V. V. Ramasesh, S. Hacohen-Gourgy, L. S. Martin, N. Y. Yao, and I. Siddiqi, Phys. Rev. X **7**, 031023 (2017).

[31] W. H. Zurek, Nature (London) **412**, 712 (2001).

[32] W. J. Munro, K. Nemoto, G. J. Milburn, and S. L. Braunstein, Phys. Rev. A **66**, 023819 (2002).

[33] J. Joo, W. J. Munro, and T. P. Spiller, Phys. Rev. Lett. **107**, 083601 (2011).

[34] W. H. Zurek, Rev. Mod. Phys. **75**, 715 (2003).

[35] M. Arndt and K. Hornberger, Nat. Phys. **10**, 271 (2014).

[36] A. Asadian, C. Brukner, and P. Rabl, Phys. Rev. Lett. **112**, 190402 (2014).

[37] K. E. Khosla, M. R. Vanner, N. Ares, and E. A. Laird, Phys. Rev. X **8**, 021052 (2018).

[38] M. Kounalakis, Y. M. Blanter, and G. A. Steele, npj Quantum Inf. **5**, 100 (2019).

[39] X. Ma, J. J. Viennot, S. Kotler, J. D. Teufel, and K. W. Lehnert, Nat. Phys. **17**, 322 (2021).

[40] J. Chen, T. Yu, C. Liu, T. Liu, M. Madami, K. Shen, J. Zhang, S. Tu, M. S. Alam, K. Xia, M. Wu, G. Gubbiotti, Y. M. Blanter, G. E. W. Bauer, and H. Yu, Phys. Rev. B **100**, 104427 (2019).

[41] T. Yu, Y.-X. Zhang, S. Sharma, X. Zhang, Y. M. Blanter, and G. E. W. Bauer, Phys. Rev. Lett. **124**, 107202 (2020).

[42] X. Zhang, G. E. W. Bauer, and T. Yu, Phys. Rev. Lett. **125**, 077203 (2020).

[43] I. Bertelli, J. J. Carmiggelt, T. Yu, B. G. Simon, C. C. Pothoven, G. E. W. Bauer, Y. M. Blanter, J. Aarts, and T. van der Sar, Sci. Adv. **6**, eabd3556 (2020).

[44] F.-X. Sun, S.-S. Zheng, Y. Xiao, Q. Gong, Q. He, and K. Xia, Phys. Rev. Lett. **127**, 087203 (2021).

[45] S. Sharma, V. A. S. V. Bittencourt, A. D. Karenowska, and S. V. Kusminskiy, Phys. Rev. B **103**, L100403 (2021).

[46] S. Sharma, V. A. Bittencourt, and S. V. Kusminskiy, arXiv:2201.10170.

[47] C. K. Law and J. H. Eberly, Phys. Rev. Lett. **76**, 1055 (1996).

[48] M. Hofheinz, H. Wang, M. Ansmann, R. C. Bialczak, E. Lucero, M. Neeley, A. O'connell, D. Sank, J. Wenner, J. M. Martinis *et al.*, Nature (London) **459**, 546 (2009).

[49] D. E. Deutsch, Proc. R. Soc. A **425**, 73 (1989).

[50] J. L. Dodd, M. A. Nielsen, M. J. Bremner, and R. T. Thew, Phys. Rev. A **65**, 040301(R) (2002).

[51] A. Parra-Rodriguez, P. Lougovski, L. Lamata, E. Solano, and M. Sanz, Phys. Rev. A **101**, 022305 (2020).

[52] C. C. Rusconi, M. J. A. Schuetz, J. Gieseler, M. D. Lukin, and O. Romero-Isart, Phys. Rev. A **100**, 022343 (2019).

[53] E. T. Jaynes and F. W. Cummings, Proc. IEEE **51**, 89 (1963).

[54] O. Shevchuk, G. A. Steele, and Y. M. Blanter, Phys. Rev. B **96**, 014508 (2017).

[55] I. Rodrigues, D. Bothner, and G. Steele, Nat. Commun. **10**, 5359 (2019).

[56] M. Kounalakis, Y. M. Blanter, and G. A. Steele, Phys. Rev. Research **2**, 023335 (2020).

[57] J. Koch, T. M. Yu, J. Gambetta, A. A. Houck, D. I. Schuster, J. Majer, A. Blais, M. H. Devoret, S. M. Girvin, and R. J. Schoelkopf, Phys. Rev. A **76**, 042319 (2007).

[58] A. B. Zorin, Phys. Rev. Lett. **76**, 4408 (1996).

[59] U. Vool and M. Devoret, Int. J. Circuit Theory Appl. **45**, 897 (2017).

[60] D. D. Stancil and A. Prabhakar, *Spin Waves* (Springer, New York, 2009), Vol. 5.

[61] See Supplemental Material at http://link.aps.org/supplemental/10.1103/PhysRevLett.129.037205 for a full derivation of the magnon-qubit system Hamiltonian and circuit quantization treatment including the role of the individual junction capacitances of the SQUID; a calculation of the critical distance between the SQUID and the magnet; and an investigation of thermal effects in the system dynamics. The Supplemental Material additionally includes Refs. [62–66].

[62] F. N. Rybakov and E. Babaev, arXiv:2203.08752.

[63] X. You, J. A. Sauls, and J. Koch, Phys. Rev. B **99**, 174512 (2019).

[64] R.-P. Riwar and D. P. DiVincenzo, npj Quantum Inf. **8**, 36 (2022).

[65] M. Popinciuc, V. E. Calado, X. L. Liu, A. R. Akhmerov, T. M. Klapwijk, and L. M. K. Vandersypen, Phys. Rev. B **85**, 205404 (2012).

[66] C. E. Murray, Mater. Sci. Eng. R Rep. **146**, 100646 (2021).

[67] M. Aspelmeyer, T. J. Kippenberg, and F. Marquardt, Rev. Mod. Phys. **86**, 1391 (2014).

[68] M. Kounalakis, Nonlinear couplings for quantum control of superconducting qubits and electrical/mechanical resonators, Ph.D. thesis, Delft University of Technology, 2019, https://doi.org/10.4233/uuid:7ffe6dfa-2a24-44d1-991f-7e1bbe2397d6.

[69] M. D. Hutchings, J. B. Hertzberg, Y. Liu, N. T. Bronn, G. A. Keefe, M. Brink, J. M. Chow, and B. L. T. Plourde, Phys. Rev. Applied **8**, 044003 (2017).

[70] N. K. Langford, R. Sagastizabal, M. Kounalakis, C. Dickel, A. Bruno, F. Luthi, D. J. Thoen, A. Endo, and L. DiCarlo, Nat. Commun. **8**, 1715 (2017).

[71] S. Klingler, H. Maier-Flaig, C. Dubs, O. Surzhenko, R. Gross, H. Huebl, S. T. B. Goennenwein, and M. Weiler, Appl. Phys. Lett. **110**, 092409 (2017).

[72] M. Kjaergaard, M. E. Schwartz, J. Braumüller, P. Krantz, J. I.-J. Wang, S. Gustavsson, and W. D. Oliver, Annu. Rev. Condens. Matter Phys. **11**, 369 (2020).

[73] L. Tian, Phys. Rev. B **72**, 195411 (2005).

[74] D. Kielpinski, D. Kafri, M. J. Woolley, G. J. Milburn, and J. M. Taylor, Phys. Rev. Lett. **108**, 130504 (2012).

[75] J.-Q. Liao, K. Jacobs, F. Nori, and R. W. Simmonds, New J. Phys. **16**, 072001 (2014).

[76] D. C. McKay, S. Filipp, A. Mezzacapo, E. Magesan, J. M. Chow, and J. M. Gambetta, Phys. Rev. Applied **6**, 064007 (2016).

[77] B. Vlastakis, G. Kirchmair, Z. Leghtas, S. E. Nigg, L. Frunzio, S. M. Girvin, M. Mirrahimi, M. H. Devoret, and R. J. Schoelkopf, Science **342**, 607 (2013).
[78] B. Vlastakis, A. Petrenko, N. Ofek, L. Sun, Z. Leghtas, K. Sliwa, Y. Liu, M. Hatridge, J. Blumoff, L. Frunzio *et al.*, Nat. Commun. **6**, 8970 (2015).
[79] J. Johansson, P. Nation, and F. Nori, Comput. Phys. Commun. **183**, 1760 (2012).
[80] J. Krause, C. Dickel, E. Vaal, M. Vielmetter, J. Feng, R. Bounds, G. Catelani, J. M. Fink, and Y. Ando, Phys. Rev. Applied **17**, 034032 (2022).
[81] G. Vidal and R. F. Werner, Phys. Rev. A **65**, 032314 (2002).
[82] M. A. Nielsen and I. L. Chuang, *Quantum Computation and Quantum Information* (Cambridge University Press, Cambridge, England, 2010).
[83] T. Hioki, H. Shimizu, T. Makiuchi, and E. Saitoh, Phys. Rev. B **104**, L100419 (2021).
[84] D. Schuster, A. Houck, J. Schreier, A. Wallraff, J. Gambetta, A. Blais, L. Frunzio, J. Majer, B. Johnson, M. Devoret *et al.*, Nature (London) **445**, 515 (2007).
[85] C. Nisoli, R. Moessner, and P. Schiffer, Rev. Mod. Phys. **85**, 1473 (2013).
[86] D. J. Weigand and B. M. Terhal, Phys. Rev. A **101**, 053840 (2020).